RESEARCH ON MOTOR LEARNING AND CONTROL OF MULTI-DOF BIONIC MANIPULATOR

Jianjun Lan*

Abstract

Motion planning of robotic systems needs to be engineered by professionals, and how to quickly and simply adjust the motion of the manipulator when external tasks change is of major importance to us. We present an action planning method by only using magnetic and inertial measurement unit (MIMU), the entire system consists of a human arm attitude measurement unit and a bionic manipulator control unit. Robotic manipulators can perform fast action learning from the pose data of the operator's arm instead of complex motion redesigns. The Kalman filter algorithm is used in inertial sensor data fusion, and the fusion of the values recorded from the inertial sensors can be decomposed into the rotation angles of the servos using a rigid body transformation using the Lie group theory. Evaluation tests were performed separately in the LabVIEW platform and on a real robotic system, and the results from the real-time tests show that the method successfully reproduces the movements performed by the operator.

Key Words

Action learning, inertial measurement unit, Kalman filter, servo control, attitude mapping

1. Introduction

Bionic manipulators could replace humans in a variety of operational tasks, such as handling and welding. With the change of tasks, the robot's motion planning needs to be redesigned by professionals [1], [2]. However, this traditional approach is cumbersome and requires a high level of skill. So many scholars have tried to use action learning methods to plan the trajectory of a robotic manipulator. In terms of action recognition, the main ways include data gloves [3], tactile sensors [4], control panels [5], visual images [6], and all kinds of wearable devices [7], and the sensors used by most of the posture detection are vision and inertial sensors. The advantage of visual sensor teleoperation is that it can make human limbs stretch naturally [8], [9], and the virtual environment through the depth camera to help the human body feel the real tactile force, to realise teleoperation [10], [11]. However, the advantage of wearable devices with multiple sensors is more pronounced in terms of real-time convenience. Many reports of the motion recognition accuracy are above 99.00% [12]–[14], and some simulations of motion tracking based on multi-sensors were performed in MATLAB [15], [16]. In terms of only using inertial sensors for motion learning, Fu *et al.* [17] presented a method based on the cubic spline to reduce the impact on the joint, and a method to limit the drift of the gyroscope was proposed in [18]. After the attitude is accurately measured, the human movement trajectory can be mapped to a robotic man manipulator using a mapping approach [18]. Though several kinematic mapping methods have been proposed, such as position mapping, joint angle mapping, pose mapping, and so on [19]–[22], those methods take a long time to compute. In [23], a method directly controlled by the robotic articulation speed has been proposed and achieved relatively good results.

This paper proposes a methodology for action learning and control of robotic manipulators using only inertial measurement units for real-time considerations and convenience. Two 9-axis inertial sensors are attached separately to the upper and lower arms of the human, and data fusion of gyroscopes, accelerometers, and magnetometers is performed using a Kalman filter fusion algorithm, which can compensate for the accuracy of pose measurements in the dynamics. After pose decomposition and mapping, the servo angle parameters of the manipulator are reconstructed using the Lie group algorithm. To verify the effectiveness of this approach, a simulation test in LabVIEW and a physical grasp test based on the KNOVA manipulator system are separately demonstrated.

2. System Framework

The structure of the system consists mainly of two parts: the arm pose detection unit and the manipulator control unit. Figure 1 shows the diagram of

* Fujian Vocational & Technical College of Water Conservancy & Electric Power, School of Electric Power Engineering, Yongan 366000, China; e-mail: licki518@163.com
Corresponding author: Jianjun Lan

Recommended by Peter Xiaoping Liu
(DOI: 10.2316/J.2024.206-0835)

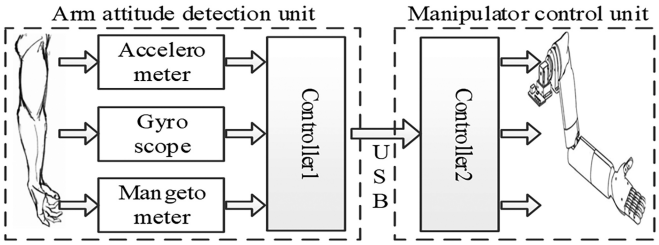

Figure 1. The structure of the system.

the system structure. In particular, the arm pose detection unit consists of controller1 as the lower computer, inertial sensors, and a USB communication interface. Two inertial sensors integrated with accelerometers, gyroscopes, and magnetometers are arranged on the upper and lower arms for human arm pose detection.

The manipulator control unit consists of controller2 as the upper computer and manipulator, which receives data from the arm pose detection unit that has been processed by controller1 into rotation angles for each servo of the manipulator. Thus controller2 can control the manipulator to mimic the movement of a human arm in real time.

3. Arm Attitude Measurements

3.1 Construction of Coordinate System

The essence of human arm attitude measurement is to construct a set of strap-down inertial navigation systems on a human arm to obtain the arm posture, position, and velocity information of the arm. Usually, the attitude information is described by the carrier coordinate system and the position information is described by the navigation coordinate system. In this study, the ENU coordinate system is selected as the navigation coordinate system (n system), and the carrier coordinate system is the b system. The b system is rotated around its Z-axis by an angle of φ, and then the new X-axis around the b system by an angle of θ. Finally, rotate the angle γ around the new Y-axis of the b system to obtain a new attitude. The schematic diagram of the rotation relationship is shown in Fig. 2 and (1).

$$\begin{bmatrix} x_b \\ y_b \\ z_b \end{bmatrix} = C_n^b \begin{bmatrix} x_n \\ y_n \\ z_n \end{bmatrix} = \begin{bmatrix} \cos\varphi & -\sin\varphi & 0 \\ \sin\varphi & \cos\varphi & 0 \\ 0 & 0 & 1 \end{bmatrix} \begin{bmatrix} 1 & 0 & 0 \\ 0 & \cos\theta & -\sin\theta \\ 0 & \sin\theta & \cos\theta \end{bmatrix} \begin{bmatrix} \cos\gamma & 0 & -\sin\gamma \\ 0 & 1 & 0 \\ \sin\gamma & 0 & \cos\gamma \end{bmatrix} \begin{bmatrix} x_n \\ y_n \\ z_n \end{bmatrix} \tag{1}$$

Where C_n^b is a rotation matrix in which each element is a directional cosine.

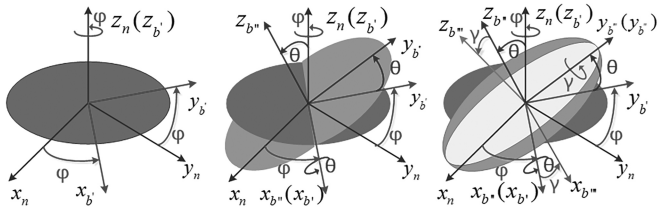

Figure 2. Schematic diagram of the rotation of two coordinate systems.

3.2 Attitude Solution

Quaternion methods are widely used for pose solutions due to their low computational cost and high accuracy. The pose solution process consists of three main parts: quaternion initialisation, quaternion update, and quaternion conversion output. The whole procedure is implemented by solving differential equations to continuously obtain new poses, and the steps are as follows:

Step 1: Quaternion initialisation
Equation (2) shows the calculation formula for the initial value of the quaternion. The initial attitude data of the human arm is needed for initialisation. Because it is impossible to ensure that the posture of the human arm is at the same position when initialised each time, the usual method is to measure a static attitude $(\varphi, \theta, \gamma)$ as the initial attitude data.

Under static conditions, the accelerometer is only affected by gravity, the yaw φ cannot be measured by the accelerometer, but only by the magnetometer, the formula is shown in (3):

$$\begin{aligned} q_0 &= \cos\frac{\gamma}{2}\cos\frac{\theta}{2}\cos\frac{\varphi}{2} - \sin\frac{\gamma}{2}\sin\frac{\theta}{2}\sin\frac{\varphi}{2} \\ q_1 &= \cos\frac{\gamma}{2}\sin\frac{\theta}{2}\cos\frac{\varphi}{2} - \sin\frac{\gamma}{2}\cos\frac{\theta}{2}\sin\frac{\varphi}{2} \\ q_2 &= \sin\frac{\gamma}{2}\cos\frac{\theta}{2}\cos\frac{\varphi}{2} + cos\frac{\gamma}{2}\sin\frac{\theta}{2}\sin\frac{\varphi}{2} \\ q_3 &= \cos\frac{\gamma}{2}\cos\frac{\theta}{2}\sin\frac{\varphi}{2} + sin\frac{\gamma}{2}\sin\frac{\theta}{2}\cos\frac{\varphi}{2} \end{aligned} \tag{2}$$

$$\varphi = \arctan\left(\frac{m_y}{m_x}\right) \tag{3}$$

Where m_x and m_y are the magnetic intensity components of the magnetometer on the X and Y axes.

When pitch θ and roll γ were only measured by the accelerometer, the attitude conversion matrix C_n^b can be simplified. Using the trigonometric function relationship, the solution results of the angle are shown in (4).

$$\begin{bmatrix} a_x^b \\ a_y^b \\ a_z^b \end{bmatrix} = \begin{bmatrix} -\mathrm{gsin}\gamma\cos\theta \\ \mathrm{gsin}\theta \\ \mathrm{gcos}\gamma\cos\theta \end{bmatrix} \Rightarrow \begin{cases} \theta = \arcsin\left(\frac{a_y^b}{g}\right) \\ \gamma = -\arctan\left(\frac{a_x^b}{a_z^b}\right) \end{cases} \tag{4}$$

Where a_x^b, a_y^b, and a_z^b are the components on the three axes of the accelerometer, and g is the acceleration due to gravity.

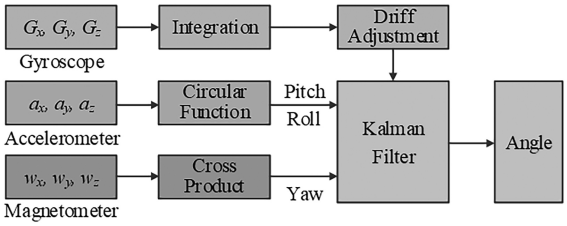

Figure 3. The principle of data fusion.

Step 2: Quaternion update
After obtaining the initial value of the quaternion, the quaternion needs to be updated continuously to obtain a continuous attitude solution. By solving differential equations of angular velocity, the solution of quaternions can be converted by (5).

$$\begin{bmatrix} \dot{q}_0 \\ \dot{q}_1 \\ \dot{q}_2 \\ \dot{q}_3 \end{bmatrix} = \frac{1}{2} \begin{bmatrix} 0 & -\omega_x & -\omega_y & -\omega_z \\ \omega_x & 0 & \omega_z & -\omega_y \\ \omega_y & -\omega_z & 0 & \omega_x \\ \omega_z & \omega_y & -\omega_x & 0 \end{bmatrix} \begin{bmatrix} q_0 \\ q_1 \\ q_2 \\ q_3 \end{bmatrix} \tag{5}$$

Where ω_x, ω_y, and ω_z are the angular velocity components of the gyroscope, q_0, q_1, q_2, and q_3 are the quaternion.

Step 3: Quaternion conversion output
Although quaternion has an advantage over Euler angle in attitude calculation, it is not intuitive in attitude description, so the output angle is expressed in the form of an Euler angle [24], the transformation relationship of the two is shown in (6).

$$\begin{aligned} \gamma &= \arctan2\left(\frac{2q_1q_2}{1-2q_2^2-2q_3^2}\right) \\ \theta &= \arcsin\left(2q_0q_2-2q_1q_3\right) \\ \varphi &= \arctan2\left(\frac{2q_2q_3+2q_0q_1}{-2q_2^2-2q_1^2+1}\right) \end{aligned} \tag{6}$$

3.3 Data Fusion and Filter

In inertial measurements, it is important to fuse the data from accelerometers, gyroscopes, and magnetometers to ensure the accuracy of the angular measurement. The Kalman filter is used as the general algorithm in this study, and Fig. 3 shows the principle of data fusion. The gyroscope is used for a prior estimate of all attitude angles, while the magnetometer is used only for yaw and the accelerometer for pitch and roll in the posterior estimate.

Firstly, the equations of linear stochastic differential and systematic observation are set up as shown in (7).

$$\begin{aligned} x_k &= Ax_{k-1} + Bu_{k-1} + w_{k-1} \\ z_k &= Hx_k + v_k \end{aligned} \tag{7}$$

Where x_k is the state value of the system at time k, A is the system transition matrix, B is the control input matrix, u_{k-1} is the input of the system at $k-1$, and w_{k-1} is the system process noise.

The optimal value estimation for the Kalman filter is a recursive filter that includes systematic predictions and measurement corrections. In the system prediction, it needs to use the posterior estimated state value $\widehat{x}_{k-1}$ at time $k-1$ to calculate the prior state estimated value $\widehat{x}_{\overline{k}}$ at time k, then calculate the prior estimated covariance $P_{\overline{k}}$. In the correction, it is necessary to dynamically adjust the Kalman gain to solve the optimal estimate with the smallest mean squared error, see Fig. 4 for the software flowchart.

4. Manipulator control

4.1 Attitude Mapping

The key to robotic arm learning from human arm motion is pose mapping, where the servos act as pivots and hinges of the manipulator, and the goal is to convert the pose data of the human arm into the rotation angle of the servos. Fig. 5 shows a schematic of the structure of the designed arm, with servos numbers 1 and 2 for the 2-DOF simulation of the upper arm, 3, 4, and 5 for the 3-DOF simulation of the lower arm, and 6 for the grasping simulation.

4.2 Attitude Decomposition and Mapping

The movement of the lower arm not only includes its own but also the driving of the upper arm. During the attitude mapping, it is necessary to construct a coordinate system for the lower arm and upper arm separately. Take the yaw for example, Fig. 6 shows the projection of the yaw on the X–Y plane. J_1 is the upper arm of the robot, J_2 is the lower arm, x^g–y^g is the upper arm coordinate system (the global coordinate system), and x^l–y^l is the lower arm coordinate system (the local coordinate system). φ_1 is the yaw of the human upper arm in the global coordinate system, and φ_2 is the yaw of the human lower arm in the global coordinate system. According to the projection transformation relationship, the yaw of the human lower arm in its local coordinate system can be calculated as $\varphi^l = \varphi_2 - \varphi_1$, which is the rotation angle of the servo.

5. System Modelling and Testing

5.1 Manipulator Modelling

The 3D model diagram of the manipulator is shown in Fig. 7, which consists of six servos (named number 1 to number 6) and relevant mechanical fasteners. The modelling process includes component sketch drawing, feature addition of the component graphics, setting up the component constraint and component assembly, and the whole process was done in SoildWorks.

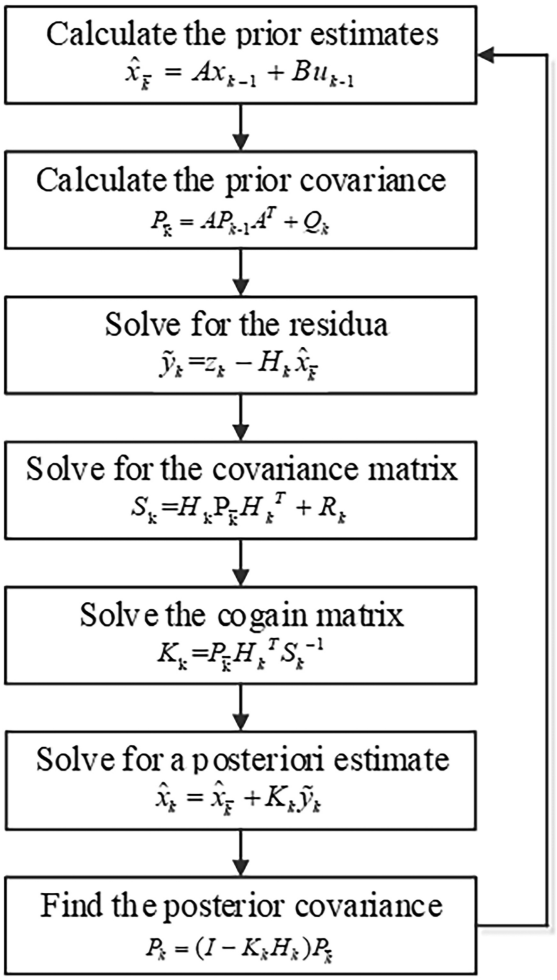

Figure 4. Flowchart of Kalman filter.

5.2 Static Data Testing

During the static test, the human arm was replaced by a manipulator because the arm could not be maintained accurately at a particular angle. The MPU9250 is fixed to the manipulator, and the servos are controlled by a single-chip microcomputer to rotate in the triaxial directions. The rotation range is 0–60°, the step is 5°. The actual angles are provided by the servo's angle which can be obtained by the conversion of the pulse width of the pulse width modulation (PWM) signal and record the measured value of the MPU9250. The test data error curve is shown in Fig. 8, and the measurement error is less than 1.5°.

5.3 Dynamic Simulation

The 3D model of the manipulator designed in SolidWorks can be imported into LabVIEW for dynamic simulation, as long as it was derived in the WRL file format. Various operations on 3D objects are supported in LabVIEW, such as relative rotation, translation, and scaling, but the independent rotation of components is not supported. Therefore, an approach that constrains the relational setting of each servo by inserting a connection point where

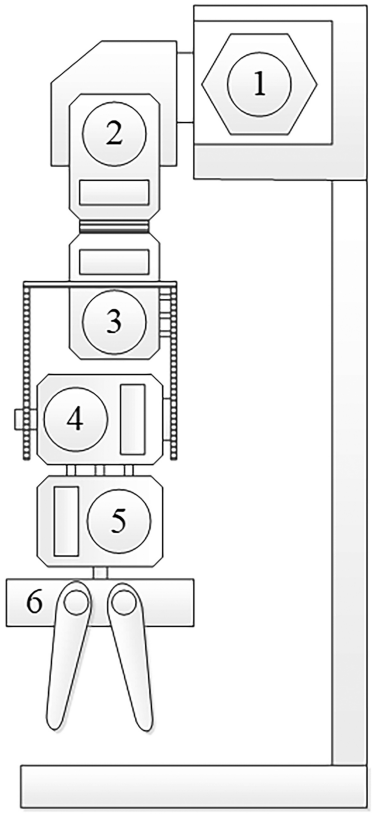

Figure 5. Structure of simulator arm.

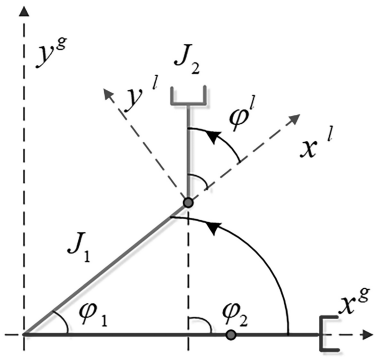

Figure 6. Yaw angle X–Y plane projection.

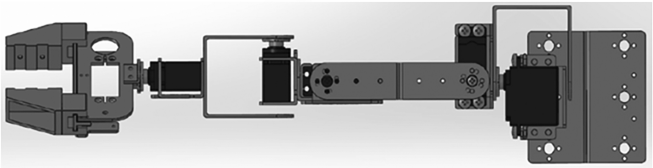

Figure 7. The 3D model diagram of the manipulator.

the rotation of the upper servo can drive the rotation of the subordinate servo is feasible for both individual and common rotations of the servos. After the design of the program panel, the VISA interface in LabVIEW is used to collect pose data of the human arm so that the robot

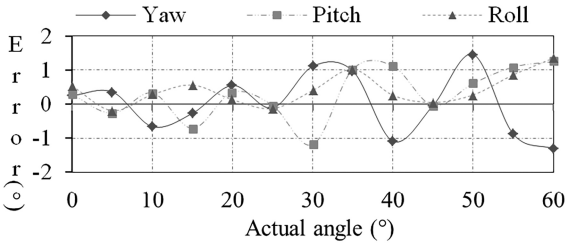

Figure 8. Absolute error curve of static test data.

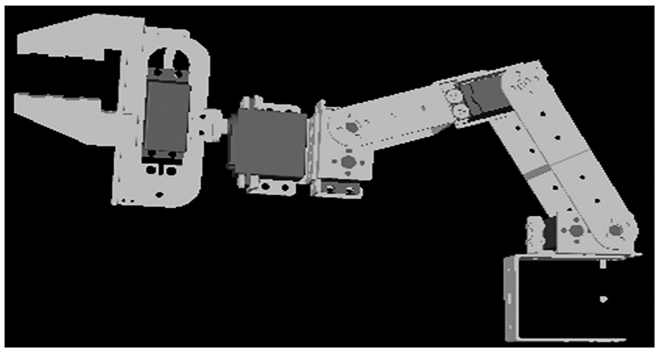

Figure 9. Dynamic motion effect of manipulator.

manipulator and the human arm can interact dynamically and synchronously, the dynamic effect is shown in Fig. 9.

6. System Implementation

We validated the presented method on an experimental platform of a KNOVA manipulator with 6-DOF. Two inertial sensors MPU9250 were used for the attitude detection of the human arm, a rheostat-type grasping control glove was used for grasping control signal detection, and a STM32 microcomputer (MCU) as the lower computer was used for the signal processing and data communication between human arm attitude detection system and KNOVA manipulator system. The experimental devices are shown in Figs. 10 and 11 which show the correspondence between the degrees of freedom of the real manipulator and the simulated manipulators in LabVIEW.

To test the effectiveness of the actual robot arm in learning human arm movements, we designed a benchmark test plane trajectory as shown in Fig. 12. The human arm moved along the plane trajectory of A–B–C such that the robot arm repeats the trajectory of the human arm. Two MPU9250 sensors were used to record the end angle changes in the X, Y, and Z-directions for the human arm and the robot arm, respectively, and the curves of the end angle changes for both arms are given in Fig. 13. The red curve is the angle change curve at the end of the human arm and the corresponding blue curve is the angle change curve at the end of the robot arm. Regardless of the need for high-precision imitation, the

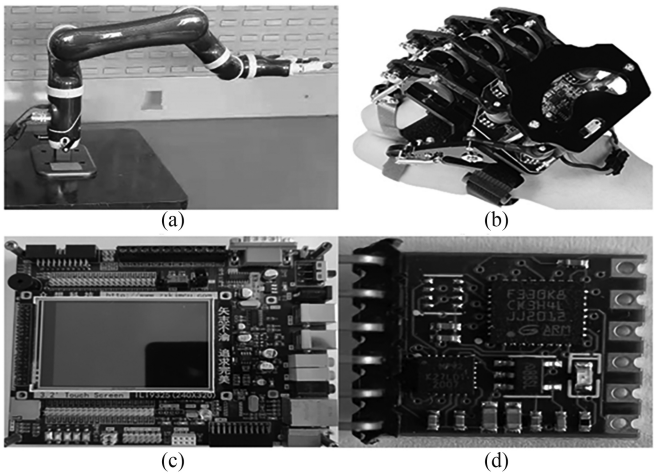

Figure 10. The relevant experimental devices: (a) KNOVA manipulator with 6-DOF; (b) grasping control glove; (c) MCU development board; and (d) MPU 9250.

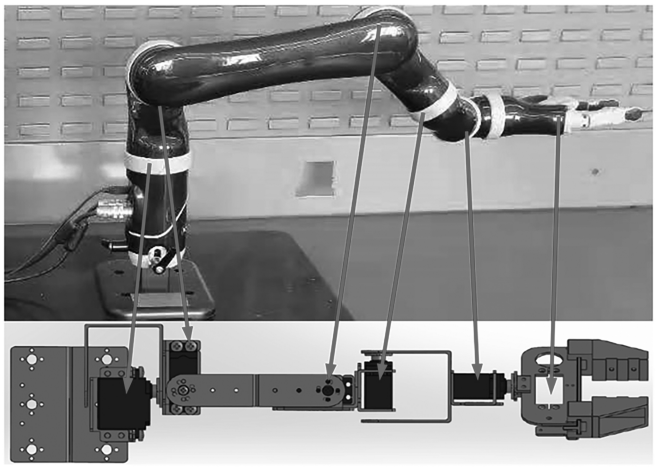

Figure 11. The corresponding relationship of the degrees of freedom between the simulated manipulator and the real manipulator.

robot arm can better reproduce the movements of the human arm.

Further, to test the effect of learning of the robot arm motion in three dimensions, we placed a plastic bottle in the workspace of the KNOVA manipulator as the grasp task target, and the glove was able to detect the degree of bending of each finger. When a grasping motion is generated, the digital signal from the MPU9250 sensor and the analog signal from the rheostat sensor can be sent to the STM32 for A/D conversion and other processing.

Figure 14 shows the entire process of grasping an object in the system. The operator continuously adjusts the posture of the real manipulator through the arm posture. After locking onto the object, the grasping action is achieved by clenching the palm and then raising the arm. Finally, the manipulator is controlled to put down the target.

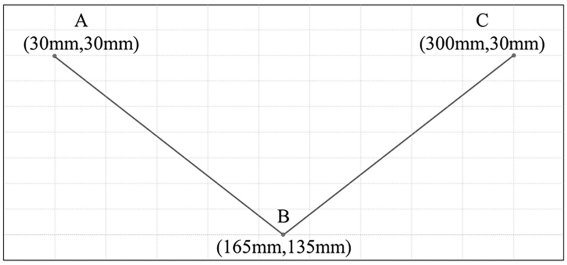

Figure 12. The benchmark test plane trajectory.

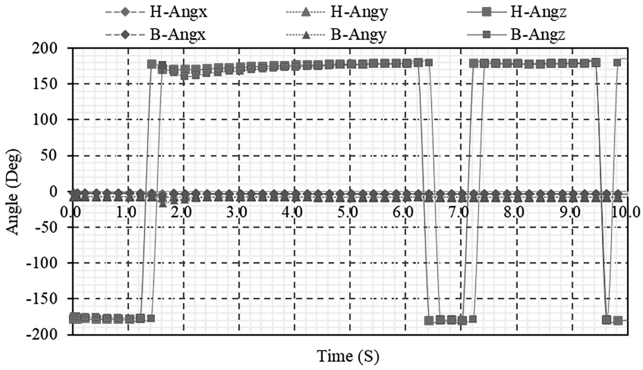

Figure 13. The comparison curve of the end angle changes.

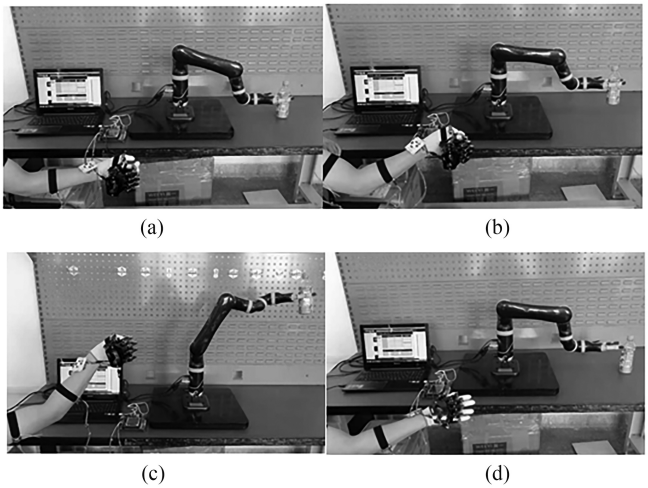

Figure 14. Grabbing object process: (a) locking the object; (b) crawl the object; (c) raise arm; and (d) put down the object.

7. Conclusion

The goal of this study is to provide an action learning method for manipulators that can quickly perform action planning using only inertial sensors. In this work, we introduce the implementation of data fusion, pose solution, and gesture mapping. This approach is cheaper than comparable methods due to its low cost and operator simplicity. We present results that demonstrate the tractability and feasibility of the proposed method for motion learning through simulation and real-world manipulation, respectively. However, the initial goal was a simple validation experiment, so the method requires further improvements, such as consideration of the length relation between the human arm and the manipulator, as well as the attitude detection and feedback of the manipulator. Subsequent research will be devoted to the improvement of the above problems and practical applications in dangerous places where robotic arms replace human arms.

References

[1] T. Guo, H. Wang, and Y. Liu, Vision-based mobile robot leader-follower control using model predictive control, *International Journal of Robotics and Automation, 34*(5), 2019, 544–552.

[2] I. Daniyan, K. Mpofu, and F. Ale, Design and simulation of a dual-arm robot for manufacturing operations in the railcar industry, *International Journal of Robotics and Automation, 36*(6), 2021, 434–447.

[3] C. Yang, X. Wang, and L. Cheng, Neural-learning-based telerobot control with guaranteed performance, *IEEE Transactions on Cybernetics, 47*(10), 2017, 3148–3159.

[4] B. Argall and A. Billard, A survey of tactile human-robot interactions, *Robotics and Autonomous Systems, 58*(10), 2010, 1159–1176.

[5] S. Günter, A. Stemmer, and R. Bischoff, The fast research interface for the KUKA lightweight robot, *Proc. 2010 IEEE Conf. on Innovative Robot Control Architectures for Demanding Applications,* Anchorage, AK, 2010, 15–21.

[6] L. Susperregi, B. Sierra, and M. Castrillón, On the use of a low-cost thermal sensor to improve kinect people detection in a mobile robot, *Sensors, 13*(11), 2013, 14687–14713.

[7] R. Jain, V.B. Semwal, and P. Kaushik, Deep ensemble learning approach for lower extremity activities recognition using wearable sensors, *Expert Systems, 16*(8), 2021, 1–17.

[8] D.H. Le and C.Y. Lin, Autonomous gluing based on image-based visual servoing, *International Journal of Robotics and Automation, 36*(2), 2021, 119–127.

[9] Z. Li, W. Yuan, and S. Zhao, Brain-actuated control of dual-arm robot manipulation with relative motion, *IEEE Transactions on Cognitive and Developmental Systems, 63*(10), 2016, 6419–6428.

[10] X. Xu, A. Song, and D. Ni, Visual-haptic aid teleoperation based on 3D environment modeling and updating, *IEEE Transactions on Industrial Electronics, 11*(1), 2017, 51–62.

[11] D. Nicolis, M. Palumbo, and A. Zanchettin, Occlusion-free visual servoing for the shared autonomy teleoperation of dual-arm robots, *IEEE Robotics & Automation Letters, 3*(2), 2018, 796–803.

[12] J. Yang, Q. Li, and X. Wang, Smart wearable monitoring system based on multi-type sensors for motion recognition, *Smart Materials and Structures, 30*(3), 2021, 612–624.

[13] A. Mukovskiy, C. Vassallo, and M. Naveau, Adaptive synthesis of dynamically feasible full-body movements for the humanoid robot HRP-2 by flexible combination of learned dynamic movement primitives, *Robotics & Autonomous Systems, 91*, 2017, 270–283.

[14] L. Roda-Sanchez, C. Garrido-Hidalgo, A. S. García, T. Olivares, and A. Fernández-Caballero, Comparison of RGB-D and IMU-based gesture recognition for human-robot interaction in remanufacturing, *International Journal of Advanced Manufacturing Technology*, *124*, 2021, 3099–3111.

[15] S. Shin, R. Tafreshi, and R. Langari, EMG and IMU based real-time HCI using dynamic hand gestures for a multiple-DoF robot arm, *Journal of Intelligent and Fuzzy Systems, 35*(1), 2018, 861–876.

[16] Y. Wei and D. Jia, Research on robotic arm movement grasping system based on MYO, *Journal of Physics: Conference Series, 1754*(1), 2021, 1–6.

[17] Y. Fu, D.S. Chen, and X.D. We, Application of optimal-jerk trajectory planning in gait balance training robot, *Chinese Journal of Mechanical Engineering, 35*(1), 2022, 61–70.

[18] Pellois R , Olivier Brüls, Human arm motion tracking using IMU measurements in a robotic environnement, *Proc. 21st*

International Symposium on Measurement and Control in Robotics, Mons, Belgium, 2018, 65–68.

[19] L. Qian, W. Hao, and W. Peng, Manipulator trajectory planning and control method based on IMU, *Proc. Conf. on Robotics, Control and Automation Engineering*, Beijing, 2018, 132–136.

[20] J. Rosell, R. Suarez, and C. Rosales, Autonomous motion planning of a hand-arm robotic system based on captured human-like hand postures, *Autonomous robots, 31*(1), 2011, 87–102.

[21] AJ. Ijspeert, J. Nakanishi, and S. Schaal, Dynamical movement primitives: Learning attractor models for motor behaviors, *Neural Comput, 25*(2), 2013, 328–373.

[22] P. Pastor, H. Hoffmann, and T. Asfour, Learning and generalization of motor skills by learning from demonstration, *Proc. IEEE Conf. on Robotics and Automation*, Kobe, 2009, 763–768.

[23] B. Fang, X. Wei, F. Sun, H. Huang, Y. Yu, and H. Liu, Skill learning for human-robot interaction using wearable device, *Tsinghua Science and Technology, 24*(6), 2019, 654–662.

[24] M.K. Özgören, Comparative study of attitude control methods based on Euler angles, quaternions, angle–axis pairs and orientation matrices, *Transactions of the Institute of Measurement and Control, 41*(5), 2019, 1189–1206.

Biography

Jianjun Lan received the B.Eng. and M.Eng. degrees in control engineering from the Northeast Electric Power University (NEEPU), China, in 2002 and 2009, respectively. He is currently an Assistant Professor with the Fujian Vocational & Technical College of Water Conservancy & Electric Power, China. He has more than twenty years of teaching and research experience and has published a number of papers in peer-reviewed conferences and international journals. His research interest includes the design of robust control, intelligent control, photoelectric detection, and new energy generation technology.